JOURNAL OF Materials CHEMISTRY

Hydrothermal synthesis and crystal structure of α-$LiZnAsO_4$

Torben R. Jensen,*[a] Poul Norby,[b]† Jonathan C. Hanson,[c] Ole Simonsen,[a] Eivind M. Skou,[a] P. C. Stein[a] and Hans A. Bøye[d]

[a]*Chemistry Department, University of Odense, DK-5230 Odense M, Denmark*
[b]*Department of Chemistry, State University of New York at Stony Brook, Stony Brook, NY11794, USA*
[c]*Chemistry Department, Brookhaven National Laboratory, Upton, NY11973, USA*
[d]*Department of Anatomy and Cytology, University of Odense, DK-5230 Odense M, Denmark*

Single crystals of lithium zinc arsenate, α-$LiZnAsO_4$, suitable for structure determination were prepared from an aqueous solution of H_3AsO_4, $Zn(NO_3)_2$ and LiOH under hydrothermal conditions, at 240 °C. α-$LiZnAsO_4$ has a fully ordered phenacite structure built from a three-dimensional framework of cornersharing AsO_4, ZnO_4 and LiO_4 tetrahedra. The tetrahedra form nets of six-rings surrounded by six four-rings in the direction of the *c*-axis. α-$LiZnAsO_4$ crystallises in the trigonal space group *R*3 (no. 146), $a = 14.009(2)$, $c = 9.386(2)$ Å, $Z = 18$ and $D_c = 3.958$ g cm^{-3}. The structure was refined to: $wR(F^2) = 0.130$, $R(F) = 0.050$ and $S = 0.982$, for $F^2 > 2\sigma(F^2)$. Synchrotron radiation, $\lambda = 0.9540$ Å, was used for single crystal diffraction giving 917 unique reflections. Solid state ^{7}Li MAS NMR showed a broadened Li signal implying more than one inequivalent Li (δ 0.21, reference: 1.00 mol dm^{-3} LiCl). Linear thermal expansion coefficients in the temperature range 25–800 °C were determined using time resolved *in situ* synchrotron X-ray powder diffraction. A weak reversible, possibly second order, thermal event was observed at 682(1) °C using differential scanning calorimetry.

A large number of microporous phosphates and some arsenates have been prepared during the last decade because of their potential catalytic properties. Introduction of lithium in this type of materials can possibly give new solid state Li ion conducting electrolytes or cathode materials.[1] The polymorph of lithium zinc arsenate, α-$LiZnAsO_4$, investigated in this study was originally prepared by a solid state reaction at 700 °C, and a phenacite type structure was proposed.[2] Recently it was shown that this polymorph could also be prepared by dehydration of $LiZnAsO_4 \cdot H_2O$.[3]

The phenacite structure, Be_2SiO_4, consists of corner sharing tetrahedra of BeO_4 and SiO_4, forming four-and six-ring channels in the *c*-direction.[4] A variety of compounds adopt the phenacite structure, *e.g.* Zn_2SiO_4 (willemite), Li_2WO_4, α-$LiGaSiO_4$, α-$LiAlSiO_4$ (α-eucryptite).[5] The name, α-$LiZnAsO_4$, is proposed for this polymorph of lithium zinc arsenate, in accordance with other isomorphous materials with similar compositions. All known phenacite type materials containing two different cations, A_2XO_4, crystallise in $R\bar{3}$, owing to formation of chains of AO_4 tetrahedra connected with discrete XO_4 tetrahedra. Phenacite type materials with three different cations are, remarkably, all lithium containing, *i.e.* $LiAXO_4$ (to the knowledge of the authors). These compounds are built from discrete tetrahedra of LiO_4, AO_4 and XO_4 sharing one corner, reducing the symmetry to *R*3. However, some refinements of $LiAXO_4$ were carried out in $R\bar{3}$ presumably because of microtwinning or disorder in the crystals. The detailed crystal structures of $LiZnVO_4$ and the solid solution $LiZn(P_xV_{1-x})O_4$, $0 < x < ca.$ 0.5, are unknown, but are proposed to be phenacite-like.[2,6] The crystal structure of the monoclinic α-$LiZnPO_4$ is related to the phenacite structure, but more complex.[7] Recently a polymorph of $LiZnPO_4$ (denoted ε-$LiZnPO_4$ in this work) was described with a fully ordered phenacite type crystal structure.[8]

We prepared lithium zinc arsenate, α-$LiZnAsO_4$, by hydrothermal synthesis for structural investigation using micro single crystal diffraction and synchrotron radiation,[9] which is presented along with thermal behaviour.

Experimental

Hydrothermal synthesis of α-$LiZnAsO_4$

In order to give a more detailed description of the formation regions of lithium zinc orthoarsenates we carried out a number of hydrothermal syntheses in the system, $H_3AsO_4 : Zn(NO_3)_2 : LiOH : H_2O$, using variable amounts of LiOH and different temperatures. A clear solution, **A**, of H_3AsO_4 (16.539 g) and $Zn(NO_3)_2$ (27.642 g) dissolved in H_2O and diluted to 100 cm^3 was prepared. The synthesis of sample **I** was performed dissolving LiOH (0.315 g) in 10 cm^3 H_2O in a Teflon lined steel autoclave. 5 cm^3 of solution **A** was added under stirring, giving a molar ratio of the reactants, $H_3AsO_4 : Zn(NO_3)_2 : LiOH : H_2O = 1.0 : 1.0 : 2.8 : \approx 175$, and $[AsO_4^{3-}] = 0.30$ mol dm^{-3}, pH = 2.5. This mixture was placed at a constant temperature of 240 °C for 43 h, the resulting yield was 0.639 g of crystalline material. Sample **I** was not phase pure but contained micro crystals usable for structure investigation.

A phase pure sample, **II**, of α-$LiZnAsO_4$ was obtained using a similar procedure, dissolving LiOH (0.448 g) in 10 cm^3 H_2O in a Teflon lined steel autoclave. 5 cm^3 of solution **A** was added under stirring, giving a molar ratio of the reactants, $H_3AsO_4 : Zn(NO_3)_2 : LiOH : H_2O = 1.0 : 1.0 : 3.9 : \approx 175$, and $[AsO_4^{3-}] = 0.30$ mol dm^{-3}, pH = 7.5. This mixture was held at a constant temperature of 240 °C for 43 h, the resulting yield was 0.948 g of crystalline material.

The syntheses were performed using the following commercial chemicals: LiOH (Merck, >98%), H_3AsO_4 (Merck, extra pure, 80%) and $Zn(NO_3)_2 \cdot 6H_2O$ (Fluka Chemie AG, purum p.a. >99.0%). The water content in lithium hydroxide was determined by thermogravimetry to 1.6% m/m. **NOTE**: Arsenic acid is highly toxic and extremely able to cause dermatitis.

† Department of Chemistry, University of Aarhus, DK-8000 Århus C, Denmark.

Table 1 Indexed powder pattern of α-$LiZnAsO_4$, $a=14.0417(6)$, $c=9.3801(8)$ Å, unit cell volume = 1601.7(2) Å^3 (38 reflections, $I/I_o>2\%$)

h	k	l	d_{calc}/Å	d_{obs}/Å	$(I/I_o)_{obs}$
1	1	0	7.0209	7.0138	16
2	0	1	5.1021	5.1082	3
1	0	2	4.3759	4.3785	13
2	1	1	4.1274	4.1281	59
3	0	0	4.0535	4.0534	24
2	0	2	3.7136	3.7160	3
2	2	0	3.5104	3.5087	72
2	1	2	3.2827	3.2837	13
3	1	1	3.1738	3.1731	11
1	1	3	2.8562	2.8552	46
4	1	0	2.6536	2.6523	100
4	0	2	2.5510	2.5506	5
2	2	3	2.3348	2.3341	27
4	2	1	2.2321	2.2324	7
5	0	2	2.1591	2.1591	9
6	0	0	2.0267	2.0258	9
5	1	2	1.9799	1.9797	4
4	3	1	1.9552	1.9558	8
5	2	0	1.9472	1.9471	12
3	3	3	1.8736	1.8732	33
5	3	0	1.7372	1.7371	4
5	3	1	1.7082	1.7085	4
6	0	3	1.7007	1.7009	7
5	0	4	1.6881	1.6884	3
6	2	1	1.6597	1.6601	4
5	2	3	1.6529	1.6525	6
7	1	0	1.6107	1.6106	14
0	0	6	1.5633	1.5632	7
6	3	0	1.5321	1.5318	9
7	1	3	1.4319	1.4322	30
5	5	0	1.4042	1.4044	7
6	3	3	1.3758	1.3759	14
9	0	0	1.3512	1.3514	6
4	1	6	1.3470	1.3470	10
7	1	5	1.2221	1.2218	3
6	6	0	1.1701	1.1698	4
8	2	4	1.1548	1.1547	3
7	1	6	1.1218	1.1218	3

Phase analysis

Optical microscopy of batch **I** revealed crystals with three distinct morphologies. By means of powder diffraction the main component of the batch, hexagonal rods with faceted ends, was identified as α-$LiZnAsO_4$. Plate like crystals (<30% m/m) and octahedra like crystals (<5% m/m) were mounted at the chemistry beamline X7B, NSLS, Brookhaven National Laboratory, USA,[10] and indexed from image plate patterns using the indexing procedures in the DENZO program[11] (further details are given later). The plate like crystals were found to be triclinic, $a=6.66$, $b=9.15$, $c=10.10$ Å, $\alpha=69.77$, $\beta=77.59$, $\gamma=76.00°$, space group $P\bar{1}$, and appeared to be a zinc arsenate hydrate with composition, $Zn_9(AsO_4)_6{\cdot}4H_2O$.[12] The octahedra like crystals were found to have an orthorhombic unit cell ($a=8.38$, $b=8.42$, $c=6.05$ Å) and were identified as the known phase, adamite $Zn_2(AsO_4)(OH)$.[13]

The indexed powder pattern of sample **II**, α-$LiZnAsO_4$, is provided in Table 1 (38 reflections, $I/I_o>2\%$). The refined hexagonal unit cell dimensions were $a=14.0417(6)$, $c=9.3801(8)$ Å, in accordance with a phenacite type structure.

Solid state NMR spectroscopy

A ^{7}Li magic angle spinning NMR spectrum of sample **II** was recorded on a Varian UNITY-500 spectrometer [11.7 T, $\nu(^7Li)=194.3$ MHz], using a Jakobsen MAS probe.[14] The sample was placed in a cylindrical rotor (Si_3N_4, 5 mm o.d., volume 220 μl). The FID was recorded with a spinning speed of 6.3 kHz and the resulting spectrum had a digital resolution of 1.2 Hz. An aqueous solution of LiCl (Merck, >99%), was used as external standard (1.00 mol dm^{-3}).

Powder X-ray diffraction

Powder diffraction data for determining and refining unit cell parameters were obtained using a Siemens D5000 diffractometer equipped with a primary Ge-monochromator (Cu-Kα_1 radiation, $\lambda=1.540\,598$ Å). A flat glass plate was used for mounting the sample. The data were collected from 5 to 90° in 2θ with a step length of 0.02° and a counting time of 12 s per step. The program CELLKANT[15] was used to refine the unit cell parameters from the observed d-spacings.

Time/temperature resolved *in situ* synchrotron X-ray powder diffraction

In order to investigate the thermal expansion of α-$LiZnAsO_4$ a newly developed *in situ* powder diffraction camera for time-, temperature- and wavelength-dependent studies was used for the data collection at beamline X7B, NSLS, Brookhaven National Laboratory, USA.[10,16] The image plate holder was mounted on the Huber diffractometer giving a 2θ range $2.9<2\theta<60.8°$ from the collected data. A stationary steel screen with a 3 mm vertical slit was placed in front of the moving image plate. The translation was performed using stepscan (900 steps) with an exposure time of 4s per step. Sample **II** was contained in an open 0.5 mm quartz glass capillary, which was rotated during the data collection. The sample was heated by a flow of hot air from 25 to 800 °C with a heating rate of 17.2 °C min^{-1}. The wavelength was determined from a powder pattern of LaB_6 to $\lambda=0.9364(1)$ Å.[17]

Differential scanning calorimetry

Differential scanning calorimetry (DSC) was performed using a SETARAM DTA 92–16.18 instrument. Sample **II** was placed in a platinum crucible and α-Al_2O_3 was used as reference. The experiment was carried out between 20 and 900 °C using a heating rate of 5 °C min^{-1} and a cooling rate of 10 °C min^{-1} in argon atmosphere. The temperature and enthalpy change calibration was carried out using the low–high quartz transition and the dehydration of gypsum, $CaSO_4{\cdot}2H_2O$.

Scanning electron microscopy

A JEOL scanning electron microscope (JSM-35CF) was used at 25 kV and medium working distance giving magnification of ×4000. The samples were pasted to brass stubs by Leit-C conductive carbon cement and after drying they were coated with 10 nm of Pt in a Balzer's sputtering coater. Sample **II** was used, both as synthesised and after two DSC experiments, *i.e.* heating to 900 °C.

Single crystal synchrotron X-ray diffraction

Data collection. Prior to data collection a single crystal of calcium fluoride, CaF_2, was mounted on the diffractometer at the chemistry beamline X7B, NSLS, Brookhaven National Laboratory, USA[10] for measuring the accurate position of the image plate (IP) as well as the zero points of the four-circle diffractometer. The data were collected using Fuji Type V image plates (200×250 mm^2) which were read using a BAS-2000 scanner with 10^4 dynamic range.

A micro single crystal of α-$LiZnAsO_4$ with dimensions, $17\times17\times60$ μm^3, from sample **I** was mounted on a glass fibre (diameter, 4 μm). The selected wavelength of the synchrotron X-rays was $\lambda=0.9540$ Å. The orientation matrix and unit cell parameters were determined from one IP. Data for structural investigation and refinement were collected with the IP holder mounted on the detector 2θ arm, $2\theta=-40°$, 106.6 mm from the crystal using ϕ-scan with a step range of $\phi_{range}=6°$ ($6°<\phi<186°$). Due to some loss of reflections along the spindle axis a hemisphere of data was not collected. A number of reflections were overexposed, and an additional data set was

Table 2 Experimental conditions and crystallographic parameters of α-$LiZnAsO_4$

crystal data			
hexagonal prism, transparent			
dimensions/μm		$17 \times 17 \times 60$	
crystal system		trigonal	
space group		$R3$ (no. 146)	
unit cell: a/Å		14.009(2)	
c/Å		9.386(2)	
V/Å^3		1595.2(5)	
Z		18	
M		211.23	
D_c/g cm^{-3}		3.958	
$F(000)$		1764	
data collection			
X7B, NSLS, Brookhaven National Laboratory, USA			
synchrotron radiation		λ/Å	0.9540
detector: image plate		T/K	293(2)
$2\theta = -40°$, $6° < \phi < 186°$		ϕ_{range}/°	6
$2\theta = 0°$, $0° < \phi < 126°$		ϕ_{range}/°	14
measured reflections		2304	
independent reflections		917	
hkl data limits		$-20 < h < 0$	
		$-12 < k < 14$	
		$-13 < l < 5$	
$\sin(\theta_{min})/\lambda$/Å^{-1}		0.067	
$\sin(\theta_{max})/\lambda$/Å^{-1}		0.728	
refinement			
full matrix on F^2			
data, parameters		915, 76	
no. reflections omitted ($F_o^2 = 0$)		2	
observed reflections [$F_o^2 > 2\sigma(F_o^2)$]		677	
weighting scheme w		$[\sigma^2(F_o^2) + (0.091P)^2]^{-1}$ $P = (F_o^2 + 2F_c^2)/3$	
absolute structure factor χ_{Flack}		0.16(4)	
$R(F)$	0.0698	$R(F)_{obs}$	0.0502
$wR(F^2)$	0.1820	$wR(F^2)_{obs}$	0.1300
S_{all}	1.167	S_{obs}	0.982
$\Delta\rho_{min}$/e Å^{-3}	−2.055	$\Delta\rho_{max}$/e Å^{-3}	1.645

Comment: the observed reflection criterion is not relevant for the refinement.

collected with the IP placed at $2\theta = 0°$ with a scan range of $\phi_{range} = 14°$ ($0 < \phi < 126°$). The exposure time for the reflections was reduced by a factor of 2 by doubling the slew speed for the rotation. Data from 39 IP were scaled together by comparison of symmetry related reflections and Lorentz polarisation correction was applied using the program DENZO[11] giving a total of 2304 intensities and a squared R-factor for the merging, $R^2_{merge} = 9.5\%$ ($R^2_{merge} = \Sigma[(I - \langle I \rangle)^2/\Sigma I^2]\%$), yielding 917 unique observations. The experimental details are given in Table 2.

Statistical comparisons between structural parameters refined from an IP data set and a data set obtained by the conventional method was performed. There was no systematic bias between the two data sets and no sign of systematic error in the two sets of refined parameters.[18]

Refinements. Direct methods, using the program SIR92,[19] in the space group $R3$, gave all the atomic positions except one oxygen and the lithium cations. The Li positions and the oxygen atom pairs were too strongly correlated through centrosymmetry to yield meaningful anisotropic thermal parameters. Attempt to refine the oxygen atoms anisotropically constrained in pairs, failed as well. The refinement (Siemens SHELXTL)[20] converged with agreement factors $wR(F^2) = 0.130$, $R(F) = 0.050$ and $S = 0.982$, for $F^2 > 2\sigma(F^2)$, with 76 parameters refined, using full matrix least squares based on F^2 (915 reflections) and a weighting scheme, $w = [\sigma^2(F_o^2) + (0.091P)^2]^{-1}$, with $P = (F_o^2 + 2F_c^2)/3$. Two reflections considered badly measured ($F_o^2 = 0$) were omitted in the refinements. The absolute structure parameter refined to $x_{Flack} = 0.16(4)$,[21] possibly due to microtwinning. Residual electron density was found close to the heavy atoms As/Zn. Scattering factors for neutral atoms were used in this refinement. The wavelength used, $\lambda = 0.9540$ Å (13.0 keV), was below the K-edge of arsenic ($\lambda = 1.044$ Å, 11.865 keV) and zinc ($\lambda = 1.283$ Å, 9.6607 keV).[22] The program FPRIME in the GSAS general structure refinement package[23] was used to estimate f' and f'' giving values at −1.493 and 3.225 for arsenic and −0.219 and 2.372 for zinc, respectively.

Statistics on the E-reflections suggested centrosymmetry: $|E| = 0.777$ (0.798, 0.886), $|E^2 - 1| = 1.047$ (0.968, 0.736), the expected mean values for centrosymmetry and non centrosymmetry, respectively, are placed in parentheses. Refinement in the centrosymmetric space group $R\bar{3}$ (no. 148) was attempted but the As/Zn distances to oxygen were intermediate to the expected As—O and Zn—O distances from known related compounds. The mean distance, As/Zn—O, was 1.802 Å, compared to mean As—O of 1.681 Å and Zn—O distance of 1.952 Å in $NaZnAsO_4$.[24] The space group $R\bar{3}$ dictates statistical distribution of As/Zn. This is violating the assumption that α-$LiZnAsO_4$ is an orthoarsenate with discrete AsO_4 tetrahedra. By lowering the space group symmetry to $R3$, an ordered As/Zn distribution can be obtained. By removing the centre of symmetry the two As/Zn positions split into four positions. Likewise the oxygen positions and the lithium position split into pairs.

Full crystallographic details, excluding structure factors (which are available from the authors on request), have been deposited at the Cambridge Crystallographic Data Centre (CCDC). See Information for Authors, *J. Mater. Chem.*, 1998, Issue 1. Any request to the CCDC for this material should quote the full literature citation and the reference number 1145/81.

Results

Atomic coordinates are given in Table 3 and selected bond lengths and bond angles are given in Table 4. Oxidation states, V_i, were calculated as a sum of bond valences.[25] The calculated oxidation states, V_i, of the cations (Table 4) are in agreement with the expected oxidation states. The calculated oxidation states of the oxygen atoms were in the range 1.91–2.10.

^{7}Li MAS NMR spectroscopy showed one broadened peak with chemical shift δ 0.21 (full width at half maximum = 374 Hz). This supports the crystallographic data which show two inequivalent Li atoms in the asymmetric unit. α-$LiZnAsO_4$ and α-$LiAlSiO_4$ are isomorphous. α-$LiAlSiO_4$ was investigated using ^{27}Al and ^{29}Si solid state MAS NMR and two inequivalent Al positions and two Si positions were found.[26] ^{7}Li MAS NMR spectroscopy was not performed on α-$LiAlSiO_4$ but two resonances are expected. ^{7}Li MAS NMR resonances are usually found to have low chemical shift resolution.

Thermal expansion of α-$LiZnAsO_4$ was investigated using

Table 3 Atomic coordinates and equivalent isotropic displacement parameters of α-$LiZnAsO_4$. $U_{(eq)}$ is defined as one third of the trace of the orthogonalized U_{ij} tensor. Isotropic displacement parameters were used for Li and O

	x	y	z	$U_{(eq)}$/Å^2
As(1)	0.1967(2)	0.2136(2)	0.8120(2)	0.0078(7)
As(2)	0.3166(2)	0.8630(2)	0.9787(2)	0.0085(8)
Zn(1)	0.2117(3)	0.0198(2)	0.9752(2)	0.0091(10)
Zn(2)	0.5264(2)	0.8808(3)	0.1427(2)	0.0096(10)
Li(1)	0.526(3)	0.873(3)	0.801(5)	0.008
Li(2)	0.214(3)	0.021(4)	0.634(5)	0.008
O(1)	0.2448(13)	0.7912(13)	0.1241(14)	0.009(3)
O(2)	0.2488(10)	0.7919(10)	0.8288(12)	0.004(2)
O(3)	0.6685(11)	0.0083(11)	0.1346(19)	0.006(4)
O(4)	0.4584(10)	0.8764(10)	0.3291(12)	0.006(2)
O(5)	0.0802(12)	0.8753(11)	0.9597(13)	0.008(3)
O(6)	0.4438(15)	0.8771(15)	0.9751(17)	0.015(4)
O(7)	0.2189(12)	0.1051(12)	0.8109(14)	0.006(3)
O(8)	0.3326(13)	0.9919(14)	0.9670(23)	0.019(5)

Table 4 Selected bond lengths (Å) and angles (°) for α-$LiZnAsO_4$. Bond valence sum, V_i, of the cations are calculated according to ref. 25[a]

As(1)−O(5)^{i}	1.682(13)	O(5)^{i}−As(1)−O(7)	108.2(7)	Zn(2)−O(3)^{vii}	1.898(14)	O(3)^{vii}−Zn(2)−O(1)^{viii}	107.1(7)
As(1)−O(7)	1.698(13)	O(5)^{i}−As(1)−O(3)^{ii}	115.6(8)	Zn(2)−O(1)^{viii}	1.92(2)	O(3)^{vii}−Zn(2)−O(6)^{ix}	108.9(7)
As(1)−O(3)^{ii}	1.705(14)	O(7)−As(1)−O(3)^{ii}	104.6(7)	Zn(2)−O(6)^{ix}	1.94(2)	O(1)^{viii}−Zn(2)−O(6)^{ix}	105.1(6)
As(1)−O(4)^{iii}	1.710(12)	O(5)^{i}−As(1)−O(4)^{iii}	110.7(7)	Zn(2)−O(4)	1.978(12)	O(3)^{vii}−Zn(2)−O(4)	109.1(6)
mean	1.70	O(7)−As(1)−O(4)^{iii}	109.4(6)	mean	1.93	O(1)^{viii}−Zn(2)−O(4)	109.8(5)
V_i	4.81	O(3)^{ii}−As(1)−O(4)^{iii}	108.0(7)	V_i	2.16	O(6)^{ix}−Zn(2)−O(4)	116.4(7)
As(2)−O(6)	1.69(2)	O(6)−As(2)−O(1)^{iv}	111.3(7)	Li(1)−O(2)^{viii}	1.86(4)	O(2)^{viii}−Li(1)−O(5)^{x}	114.0(22)
As(2)−O(1)^{iv}	1.696(15)	O(6)−As(2)−O(8)	107.5(8)	Li(1)−O(5)^{x}	1.89(5)	O(2)^{viii}−Li(1)−O(3)^{xi}	105.3(20)
As(2)−O(8)	1.71(2)	O(1)^{iv}−As(2)−O(8)	113.8(8)	Li(1)−O(3)^{xi}	1.93(4)	O(5)^{x}−Li(1)−O(3)^{xi}	108.3(23)
As(2)−O(2)	1.711(12)	O(6)−As(2)−O(2)	107.3(7)	Li(1)−O(6)	2.01(5)	O(2)^{viii}−Li(1)−O(6)	104.6(23)
mean	1.70	O(1)^{iv}−As(2)−O(2)	109.0(7)	mean	1.92	O(5)^{x}−Li(1)−O(6)	114.3(20)
V_i	4.77	O(8)−As(2)−O(2)	107.7(8)	V_i	1.18	O(3)^{xi}−Li(1)−O(6)	110.0(20)
Zn(1)−O(8)^{v}	1.92(2)	O(8)^{v}−Zn(1)−O(7)	108.5(8)	Li(2)−O(8)^{xii}	1.89(4)	O(8)^{xii}−Li(2)−O(1)^{vi}	106.8(20)
Zn(1)−O(7)	1.922(13)	O(8)^{v}−Zn(1)−O(5)^{v}	104.9(6)	Li(2)−O(1)^{vi}	1.91(5)	O(8)^{xii}−Li(2)−O(4)^{vi}	108.9(21)
Zn(1)−O(5)^{v}	1.945(14)	O(7)−Zn(1)−O(5)^{v}	108.4(6)	Li(2)−O(4)^{vi}	1.96(4)	O(1)^{vi}−Li(2)−O(4)^{vi}	113.8(23)
Zn(1)−O(2)^{vi}	1.981(12)	O(8)^{v}−Zn(1)−O(2)^{vi}	110.1(7)	Li(2)−O(7)	2.02(5)	O(8)^{xii}−Li(2)−O(7)	107.6(22)
mean	1.94	O(7)−Zn(1)−O(2)^{vi}	115.7(6)	mean	1.95	O(1)^{vi}−Li(2)−O(7)	115.5(21)
V_i	2.11	O(5)^{v}−Zn(1)−O(2)^{vi}	108.7(5)	V_i	1.11	O(4)^{vi}−Li(2)−O(7)	104.0(20)

[a]Symmetry transformations used to generate equivalent atoms: (i) $-y+1,x-y+1,z$, (ii) $-y+1/3,x-y-1/3,z+2/3$, (iii) $x-1/3,y-2/3,z+1/3$, (iv) $x,y,z+1$, (v) $x,y-1,z$, (vi) $-x+y-1/3,x+1/3,z+1/3$, (vii) $x,y+1,z$, (viii) $-x+y,-x+1,z$, (ix) $x,y,z-1$, (x) $-y+4/3,x-y+5/3,z-1/3$, (xi) $-x+y+4/3,-x+5/3,z+2/3$, (xii) $-y+4/3,x-y+2/3,z-1/3$.

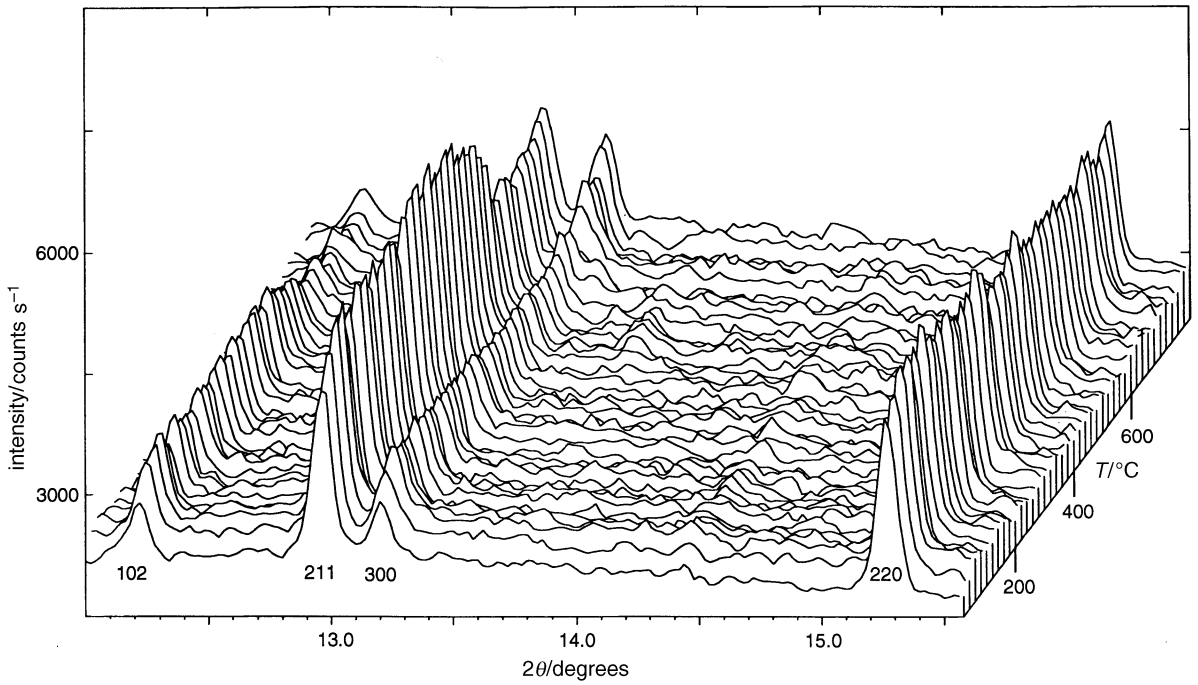

Fig. 1 Three-dimensional *in situ* powder diffraction patterns of α-$LiZnAsO_4$ as a function of time/temperature, using synchrotron radiation and an image plate area detector, in the temperature range 20–800 °C

in situ synchrotron X-ray powder diffraction. Fig. 1 shows a part of the powder patterns where a change in intensity can be observed for some of the reflections at $T>400$ °C. The unit cell parameters were refined and the temperature dependence is illustrated in Fig. 2. The linear thermal expansion coefficients of α-$LiZnAsO_4$ were calculated using the equation: $\alpha_L=(1/L_o)(\Delta L/\Delta T)$ where L denotes a unit cell axis or volume and L_o is the extrapolated value, at 0 °C. The results are found in Table 5. The linear thermal expansion coefficients increases, at 400 °C, and the thermal expansion of the *c*-axis shows a larger change than the *a*-axis. Differential scanning calorimetry is shown in Fig. 3. The DSC experiment was performed twice using the same sample. The upper curve is the first heating, the middle curve is the second heating and the lower curve is one of the similar cooling curves. A reversible thermal event with onset temperatures at 682(1) and 676(1) °C, heating and cooling, respectively is shown in Fig. 3. This event is mainly a change in baseline of the monitored DSC signal, suggesting that only a change in heat capacity is taking place. An unidentified small irreversible exothermic event is found to occur with onset at 517(1) °C and an enthalpy change of $\Delta H=-6(2)$ J g^{-1}.

Table 5 Linear unit cell expansion coefficients of α-$LiZnAsO_4$ calculated from *in situ* powder diffraction data

temperature range/°C	*a*-axis $\alpha_a/10^{-5}$ K^{-1}	*c*-axis $\alpha_c/10^{-5}$ K^{-1}	volume $\alpha_{Volume}/10^{-5}$ K^{-1}
20–400	0.91	1.1	2.9
400–800	1.2	1.8	4.1

Discussion

Description of the α-$LiZnAsO_4$ structure and the thermal behaviour

The single crystal data along with solid state ^{7}Li MAS NMR demonstrated that this polymorph of lithium zinc arsenate has

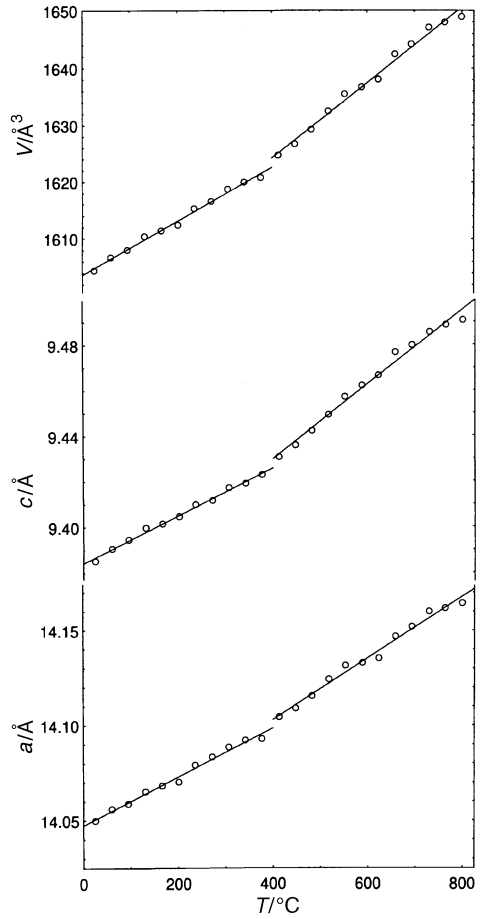

Fig. 2 Thermal expansion of the unit cell parameters of α-$LiZnAsO_4$, in the temperature range 20–800 °C

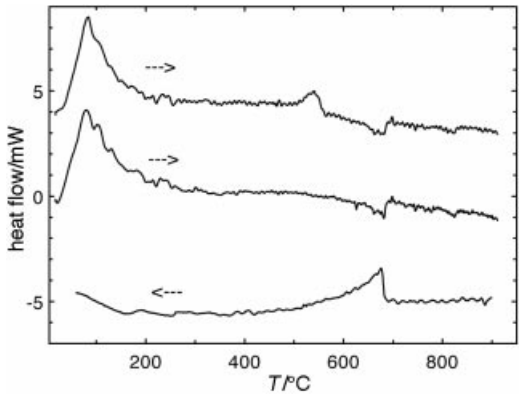

Fig. 3 Differential scanning calorimetry of α-$LiZnAsO_4$ between 20 and 900 °C. The upper curve is the first heating, the middle curve is the second heating and the lower curve is one of the similar cooling curves.

the $R3$ symmetry. The apparent centrosymmetry ($R\bar{3}$) is caused by the heavy atoms, As and Zn, having similar diffraction efficiency.

The structure refinement revealed a fully ordered phenacite type structure of α-$LiZnAsO_4$. Cation ordering in the crystal structure results in relatively regular AsO_4, ZnO_4 and LiO_4 tetrahedra. The structure of this lithium zinc arsenate can be viewed as a three-dimensional framework built from cornersharing AsO_4, ZnO_4 and LiO_4 tetrahedra. Each oxygen atom is nearly planar trigonally coordinated to Li, Zn and As. Fig. 4 show the crystal structure of α-$LiZnAsO_4$ viewed along the *c*-axis with the characteristic stacking of nets of six- and four-rings of tetrahedra of AsO_4, ZnO_4 and LiO_4. The cations

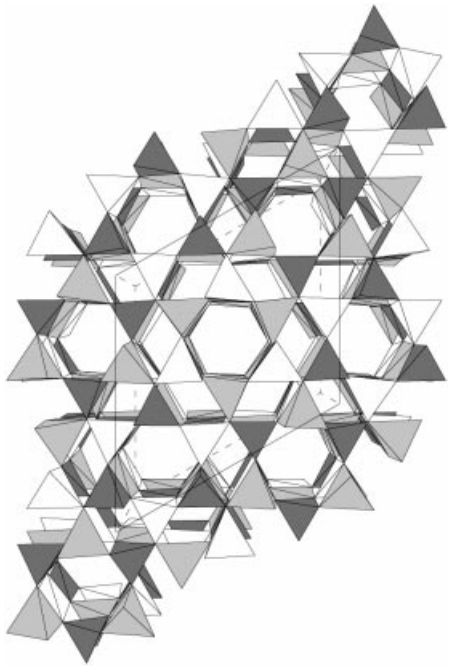

Fig. 4 The crystal structure of α-$LiZnAsO_4$ viewed along the *c*-axis, showing the phenacite like nets with six- and four-rings of tetrahedra. AsO_4 dark shaded, ZnO_4 light shaded and LiO_4 as medium shaded tetrahedra.

are stacked alternatingly with the sequence, ABCA, in columns parallel to the *c*-axis.

In situ synchrotron X-ray powder diffraction up to 800 °C indicates only minor structural changes and only variation in intensity of some reflections, *i.e.* no discontinuity in the unit cell volume (see Fig. 1). The linear thermal expansion coefficients increase abruptly at 400 °C, *i.e.* discontinuity in the first derivative of the unit cell volume (see Fig. 2). This might be a premonitory effect of the reversible change in heat capacity found by DSC (see Fig. 3). The observed phase transition thus shows second order behaviour, using a thermodynamic classification (see ref. 27).

Scanning electron microscopy was carried out for characterisation of the material (sample **II**) before and after the DSC experiments. Fig. 5(*a*) reveals crystals of α-$LiZnAsO_4$ (hexagonal rods) with dimensions of *ca.* $0.5 \times 0.5 \times 5$ μm^3, and a few larger crystals of *ca.* $2 \times 2 \times 12$ μm^3. Very few ball like unidentified particles, with diameter *ca.* 1 μm, were observed. After heating sample **II** to 900 °C twice, Fig. 5(*b*), this material could be identified as α-$LiZnAsO_4$ using powder X-ray diffraction. However the morphology of the material has changed dramatically. The product, Fig. 5(*b*), was sintered to form an agglomerate with no visible crystal facets.

Comparison with related materials

Table 6 shows selected oxides with phenacite structure. All phenacite related materials have a cation : anion ratio of 3 : 4. This includes Li_2BeF_4 and the phenacite related compounds Si_3N_4 and Ge_3N_4.[28] All known phenacite type compounds with two different cations (*e.g.* A_2XO_4) crystallise in $R\bar{3}$, independently of the effective cationic radii. The phenacite structure of A_2XO_4 materials can be viewed as layers of cations in the direction of the *c*-axis, with an AO_4 and XO_4 stacking sequence ABAB. These layers consist of tetrahedra forming six-rings of alternating AO_4 and XO_4 tetrahedra surrounded by six four-rings, giving infinite chains of AO_4 tetrahedra (in the *c*-direction) held together by distinct XO_4 tetrahedra.

Phenacite related compounds containing three different cations, *e.g.* $LiAXO_4$, tend to crystallise with lower symmetry, $R3$, giving the oxygen atoms a nearly planar trigonal coordi-

Fig. 5 Scanning electron microscopy photographs of α-$LiZnAsO_4$, (*a*) as synthesised (top) and (*b*) after two DSC experiments, heating to 900 °C. Magnification, × 4000.

nation to one Li, A and X atom each. This is meeting the valence requirement of the oxygen atoms giving fully ordered phenacite structures, *e.g.* α-$LiZnAsO_4$, α-$LiGaSiO_4$[5c] and ε-$LiZnPO_4$.[8] The cation positions of the phenacite type materials were denoted T_1, T_2 and T_3, where the T_1 position has pseudo-centrosymmetry and is the Si position in the structure of Be_2SiO_4. Table 6 reveals a characteristic trend in the cation radius ratio, $r(T_2)/r(T_3)$, of $LiAXO_4$ materials, also mentioned in ref. 5(*c*). The ratios were calculated using effective ionic radii from ref. 29. A cationic radius ratio >1.5 facilitates fully ordered phenacite structure.

α-Eucryptite, α-$LiAlSiO_4$, has a cation radius ratio $r(T_2)/r(T_3)=1.50$, and the structure was refined in the space group $R\bar{3}$. The apparent high symmetry was suggested to be due to statistical distribution of Al/Si on the T_2/T_3 positions.[5d] It was found using ^{27}Al and ^{29}Si solid state MAS NMR that there are two inequivalent Al positions and two Si positions in the asymmetric unit.[26] This suggests that the true space group is $R3$ with a fully ordered Al/Si distribution, and that the refinement was successfully performed in $R\bar{3}$ due to micro-twinning with small fully ordered domains.

The detailed structures of α-$LiGaGeO_4$ and α-$LiAlGeO_4$ remain unclear. The existence of micro structures with ordered domains remains a possibility.[5c] Disordering on the T_2/T_3 positions introduces imbalance in the sum of electrostatic bond strengths of the oxygen atoms. This imbalance is less pronounced if Li is in the T_1 position and if the cations in T_2/T_3 have oxidation states which are not too different, *e.g.* a difference of one Al/Ge or Ga/Ge. A degree of disorder might be found in α-$LiAlGeO_4$ and α-$LiGaGeO_4$ also due to the low ratios of cationic radii, 1.00 and 1.21, respectively.[5c]

The oxidation states of lithium and zinc differ by one and these two ions have very similar bond lengths to oxygen, suggesting the possibility of a degree of disorder. Statistical distribution of Li and Zn was found in silicates and germanates.[30] By means of Rietveld refinement of powder X-ray diffraction data, an indication of disorder was found in the cristobalite type polymorph, δ_l-$LiZnPO_4$.[31] No sign of disorder was found in the crystal structures of α-$LiZnAsO_4$ and ε-$LiZnPO_4$, likely because Li occupies the T_1 position in α-$LiZnAsO_4$ and Zn occupies the T_1 position in ε-$LiZnPO_4$. The relatively large difference in oxidation state and cationic radius ratio, $r(T_2)/r(T_3)$, on the T_2 and T_3 positions (see Table 6), forces fully ordered phenacite type crystal structures of α-$LiZnAsO_4$ and ε-$LiZnPO_4$. This matches the valence requirement of the oxygen atoms.

Conclusion

Hydrothermal synthesis of micro single crystals of lithium zinc arsenate, α-$LiZnAsO_4$, suitable for refinement of the fully ordered phenacite structure is reported. Linear thermal expansion coefficients in the temperature range 25–800 °C were determined using time/temperature resolved *in situ* synchrotron X-ray powder diffraction. A change in the thermal expansion coefficients occurs at 400 °C and a change in some intensities in the powder patterns suggests a small structural change. These observations, combined with differential scanning calorimetry, suggest a second order reversible phase transition.

We gratefully acknowledge R. G. Hazell, University of Aarhus for helpful discussions. The research carried out at the National Synchrotron Light Source at Brookhaven National Laboratory is supported under contract DE-AC02–76CH00016 with the US Department of Energy by its Division of Chemical Science, Office of Basic Energy Science. The Danish Technical Research Council and the Danish Natural Science Research Council are thanked for support.

Table 6 Selected oxides adopting the phenacite structure. Cationic radius ratios, $r(T_2)/r(T_3)$, are calculated, using ref. 29

	a_h/Å	c_h/Å	space group	T_1	T_2/T_3	$r(T_2)/r(T_3)$	ref.
$LiAXO_4$							
ε-$LiZnPO_4$	13.628(3)	9.096(2)	$R3$	Zn	Li/P	3.47	8
α-$LiGaSiO_4$	13.643(1)	9.0965(7)	$R3$	Ga	Li/Si	2.27	5(*c*)
α-$LiZnAsO_4$	13.923(2)	9.395(2)	$R3$	Li	Zn/As	1.79	
α-$LiAlSiO_4$	13.471(3)	8.998(2)	$R\bar{3}$(?)	Li	Al/Si	1.50	5(*d*)
α-$LiGaGeO_4$	13.9357(6)	9.2957(4)	$R\bar{3}$(?)	Li	Ga/Ge	1.21	5(*c*)
α-$LiAlGeO_4$	13.7683(9)	9.1919(5)	$R\bar{3}$(?)	Li	Al/Ge	1.00	5(*c*)
A_2XO_4							
Be_2SiO_4	12.472	8.252	$R\bar{3}$	Si	Be	1	4
Zn_2SiO_4	13.948(2)	9.315(2)	$R\bar{3}$	Si	Zn	1	5(*a*)
Li_2WO_4	14.361(3)	9.602(2)	$R\bar{3}$	W	Li	1	5(*b*)

References

1 S. R. S. Prabaharan, M. S. Michael, S. Radhakrishna and C. Julien, *J. Mater. Chem*., 1997, **7**, 1791.
2 A. Durif, *Bull. Soc. Fr. Minéral. Cristallogr*., 1961, **84**, 322.
3 T. E. Gier and G. D. Stucky, *Nature* (*London*), 1991, **349**, 508.
4 (*a*) W. L. Bragg and W. H. Zachariasen, *Z. Kristallogr*., 1930, **72**, 518; (*b*) W. H. Zachariasen, *Sov. Phys.-Crystallogr. (Engl. Transl.)*, 1972, **16**, 1021.
5 (*a*) K.-H. Klaska, J. C. Eck and D. Pohl, *Acta Crystallogr., Sect. B,* 1978, **34**, 3324; (*b*) W. H. Zachariasen and H. A. Plettinger, *Acta Crystallogr*., 1961, **14**, 229; (*c*) M. E. Fleet, *Z. Kristallogr*., 1987, **180**, 63; (*d*) K.-F. Hesse, *Z. Kristallogr*., 1985, **172**, 147.
6 G. Torres-Trevino, Ph.D. Thesis, University of Aberdeen, 1986.
7 (*a*) G. Torres-Trevino and A. R. West, *J. Solid State Chem*., 1986, **61**, 56; (*b*) L. Elammari and B. Elouadi, *Acta Crystallogr., Sect. C,* 1989, **45**, 1864.
8 Xianhui Bu, T. E. Gier and G. D. Stucky, *Acta Crystallogr., Sect. C,* 1996, **52**, 1601.
9 T. R. Jensen, P. Norby and J. C. Hanson, NSLS Activity Report 1996, BNL 52517, Brookhaven National Laboratory, Upton, NY, 1996, p. B-78.
10 (*a*) N. F. Gmur, *NSLS users manual: Guide to the VUV and X-ray Beamlines*, Informal Report 48724, 5th edn., Brookhaven National Laboratory, Upton, NY, 1993; (*b*) J. B. Hastings, P. Suortti, W. Thomlinson, A. Kvick and T. F. Koetzle, *Nucl. Instrum. Methods*, 1983, **208**, 55.
11 W. Minor, XDISPLAYF, Purdue University, 1993; Z. Otwinowski, Oscillation Data Reduction Program, Compiled by L. Sawyer in *Proceedings of the CCP4 study weekend: Data collection and Processing*, 29–30 January 1993, p. 56.
12 (*a*) T. R. Jensen, P. Norby and J. C. Hanson, NSLS Activity Report 1996, BNL 52517, Brookhaven National Laboratory, Upton, NY, 1996, p. B-79; (*b*) Pingyun Feng, Xianhui Bu and G. D. Stucky, *Acta Crystallogr., Sect. C,* 1997, **53**, 997; (*c*) T. R. Jensen, P. Norby, J. C. Hanson, E. M. Skou and P. C. Stein, *J. Chem. Soc., Dalton Trans*., in press.
13 R. J. Hill, *Am. Mineral*., 1976, **61**, 979.
14 H. J. Jakobsen, P. Daugaard and V. Langer, *J. Magn. Reson*., 1988, **76**, 162; *US Pat*., 4 739 270, 1988.
15 N. O. Ersson, CELLKANT, Program for unit cell refinement from powder diffraction data, Chemical Institute, Uppsala University, Uppsala, 1981.
16 (*a*) P. Norby, *J. Appl. Crystallogr*., 1997, **30**, 21; (*b*) *Materials Science Forum*, 1996, **228–231**, 147.
17 (*a*) P. Norby, *J. Am. Chem. Soc*., 1997, **119**, 5215; (*b*) A. N. Christensen, P. Norby, J. C. Hanson and S. Shimada, *J. Appl. Crystallogr*., 1996, **29**, 265; (*c*) A. N. Christensen, P. Norby and J. C. Hanson, *J. Solid State Chem*., 1995, **114**, 556.
18 T. Gasparik, J. B. Parise, B. A. Eiben and J. A. Hriljac, *Am. Mineral*., 1995, **80**, 1269.
19 A. Altomare, G. Cascarano, C. Giacovazzo, A. Guagliardi, M. C. Burla, G. Polidori and M. J. Camalli, *J. Appl. Crystallogr*., 1994, **27**, 435.
20 G. M. Sheldrick, SHELXTL, Siemens Analytical X-ray Systems Inc., Madison, WI, 1995.
21 H. D. Flack, *Acta Crystallogr., Sect. A,* 1983, **39**, 876.
22 (*a*) A. J. C. Wilson, *International Tables for Crystallography*, Kluwer, Dordrecht, 1992, vol. C; (*b*) D. R. Lide, *CRC Handbook of Chemistry and Physics*, 74th edn., CRC Press, Boca Raton, FL, 1993.
23 (*a*) D. T. Cromer, *J. Appl. Crystallogr*., 1983, **16**, 437; (*b*) A. C. Larson and R. B. Von Dreele, GSAS, General Structure Analysis System, Report LAUR 86–748, Los Alamos National Laboratory, NM, 1994.
24 M. Andratschke, K.-J. Range and U. Klement, *Z. Naturforsch., Teil B,* 1993, **48**, 965.
25 I. D. Brown and D. Altermatt, *Acta Crystallogr., Sect. B,* 1985, **41**, 244.
26 P. Norby, Ph.D. Thesis, Aarhus Universitet, 1989.
27 A. R. West, *Solid State Chemistry and its Applications*, Wiley, Chichester, 1984, ch. 12.3.
28 (*a*) J. H. Burns and E. K. Gordon, *Acta Crystallogr*., 1966, **20**, 135; (*b*) A. F. Wells, *Structural Inorganic Chemistry*, Clarendon Press, Oxford, 5th edn., 1984, p. 89; (*c*) R. Grün, *Acta Crystallogr., Sect. B,* 1979, **35**, 800.
29 R. D. Shannon, *Acta Crystallogr., Sect. A,* 1976, **32**, 751.
30 (*a*) Shu-Cheng Yu, D. K. Smith and S. B. Austerman, *Am. Mineral*., 1978, **63**, 1241; (*b*) W. H. Baur, *Inorg. Nucl. Chem. Lett*., 1980, **16**, 525.
31 T. R. Jensen, P. Norby, P. C. Stein and A. M. T. Bell, *J. Solid State Chem*., 1995, **117**, 39.

Paper 7/07130B; *Received* 2*nd October*, 1997